J Mater Sci: Mater Electron (2026) 37:294

Synthesis and characterization of iron interlayers as modulators of optical and dielectric performance in ZnO thin films

S. S. Fouad[1], A. E. Bekheet[1], E. Barádacs[2,3], M. Nabil[4,*], G. Vecsei[2], G. katona[2], and Z. Erdélyi[2]

[1] *Department of Physics, Faculty of Education, Ain Shams University, Cairo 11566, Egypt*
[2] *Department of Solid-State Physics, Faculty of Science and Technology, University of Debrecen, P.O. Box400, Debrecen 4002, Hungary*
[3] *Department of Environmental Physics, University of Debrecen, Poroszlay U.6, Debrecen 4026, Hungary*
[4] *Department of Basic Engineering Sciences, Faculty of Engineering (Shoubra), Benha University, Benha, Egypt*

Received: 9 September 2025
Accepted: 3 January 2026

ABSTRACT

This work explores the influence of Fe interlayer thickness on the morphology, optical, and dielectric behavior of ZnO-based multilayer film prepared by a combined ALD-DC technique. Morphology was analyzed using focused ion beam (FIB) and energy-dispersive X-ray spectroscopy (EDX), while optical properties were evaluated through transmittance and reflectance measurements. The prepared lamellae confirmed well-defined thickness of each individual layer, and (EDX) confirmed the absence of other elements present in the thin-film samples under study. According to the results presented in the obtained figures, the increase of the Fe thickness in ZnO/Fe/ZnO system leads to a decrease in transmittance and an increase in reflectance, refractive index (n), extinction coefficient (k), and reflectivity (R_{ref}). Both the real and imaginary parts of the dielectric constant (ε_1 & ε_2), as well as the dielectric loss ***(tanδ)*** increases with Fe content, while the optical quality factor ***(Q)*** decreases. Moreover, the carrier concentration to effective mass ratio ***(N/m^*)*** and both optical and electrical conductivity ***(σ_{opt} & σ_{elec})*** increases, whereas the electrical modulus **(M^*)** decreases with increasing Fe thickness**.** The Wemple-DiDomenico single-oscillator **(WDD)** model was employed to determine the dispersion parameters, from which the nonlinear refractive index ***(n_2)*** and third-order nonlinear susceptibility **($X^{(3)}$)** was estimated. These results highlight the significant role of Fe in tailoring the optical and dielectric properties of ZnO-based opto-electronics applications.

Address correspondence to E-mail: mohammed_diab35@yahoo.com

https://doi.org/10.1007/s10854-026-16594-5
Published online: 02 February 2026

1 Introduction

Among various oxide semiconductors zinc oxide (ZnO) has emerged as one of the most promising materials because of its outstanding optical transparency, electrical conductivity and chemical stability. It is now considered as a commercially active channel material in a wide range of applications, such as nanotechnology, light emitting diode, optical switches, and photonic devices, because, it has a wide direct bandgap (≈ 3.3 eV) and high exciton binding energy (60 meV) and high chemical stability, low toxicity, and high transparency in the visible wavelength [1, 2]. Modification of ZnO by various metal or metal oxide is multifaceted, influencing its structural, optical and electrical characterization, affecting its surface area and reactivity, can also influence the morphology of ZnO nanostructure. Metallic layers can develop and optimize the thin-film process for controlling and improving the efficiencies of optoelectronic devices by reducing their band gap leading to shift of the luminescence that can impact on the crystallinity of ZnO, alter the grain size, and can increase their conductivity [3, 4]. Transparent conductive ZnO films with high visible transmittance could be realized by the addition of metals, such as Cu, Ni, Mn, In, and Ti [5–8]. The introduction of Fe as an interlayer in the ZnO-based system is motivated by the unique physical and chemical characteristics. Iron, as a transition metal, possesses partially filled d-orbitals that can strongly interact with the ZnO matrix, leading to modifications in electronic structure, defect density, and carrier concentration. Moreover, Fe incorporation influenced the refractive index, absorption, and reflectance, as well as enhanced the electrical conductivity due to the possible formation of Fe^{2+}/Fe^{3+} mixed states. These combined effects make Fe a promising candidate for improving the performance of ZnO-based multilayer structure in optoelectronic and photonic applications [9–12]. Several methods are used for the synthesis of ZnO thin films using spray pyrolysis, roll-to-roll, printing sol–gel, laser ablation, and sputter deposition [13–16]. Recently, atomic layer deposition ALD and DC magnetron sputtering have attracted significant interest as an attractive method for preparing layer-by-layer thin film. The ALD enables the deposition of uniform and conformal thin films, allows for precise control over film thickness and can be performed at relatively low temperature, reducing thermal stress and damage to the substrate, while the DC magnetron sputtering offers high deposition rates, good film uniformity, control over film property such as thickness and microstructure and can also be performed at low substrate temperature as well. That's why they appear to be the perfect techniques to grow our ZnO/Fe/ZnO thin-film samples, in order to overcome the new technological challenges [17–20]. The present work is devoted to understanding how Fe incorporation can effectively modulate the structural arrangement, optical response, and dielectric functionality of ZnO, providing valuable insight into optimizing its performance for potential optoelectronic applications [21, 22]. To achieve this optical characteristic of ZnO/Fe/ZnO thin films, including their dielectric behavior, optical conductivities, and refractive indices (both linear and nonlinear) were evaluated using the Wemple–DiDomenico model. This investigation is motivated by the desire to elucidate how varying Fe thickness influences and improved the overall performance of ZnO.

2 Thin film preparation

The ZnO/Fe/ZnO thin films with varying Fe contents in the form of (80 nm/(20, 40, 60, 80 nm)/80 nm) were prepared using a combination of ALD and magnetron sputtering equipment. First, 80-nm ZnO was grown on the substrates by ALD (Beneq TFS-200). Subsequently, Fe layers of different thicknesses (20, 40, 60, 80 nm nominal thickness) were grown on the ZnO layer by magnetron sputtering. Then, 80-nm ZnO layer was deposited again on top of the Fe layers by ALD method. ZnO layers were prepared at 200 ◦C using water (H_2O) and diethylzinc (DEZ) precursors. The H_2O and DEZ pulses were 300 ms long, while the purge time was 3 s in all cases. In total, 444 cycles were used to grow 80-nm ZnO. During the deposition of the Fe layers by magnetron sputtering, the chamber pressure was 6.3×10^3 mbar and the sputtering power used was 24 W. A detailed description of the preparation process of the ZnO/Fe/ZnO samples with different thickness of Fe, covering all aspects, can be found in the following references [22, 23] and is further illustrated by Fig. 1, and providing a clear guide for reproducibility. The thin film samples in this study will be labeled as $ZF_{20}Z$, $ZF_{40}Z$, $ZF_{60}Z$, and $ZF_{80}Z$. The transmittance and reflectance spectra were recorded

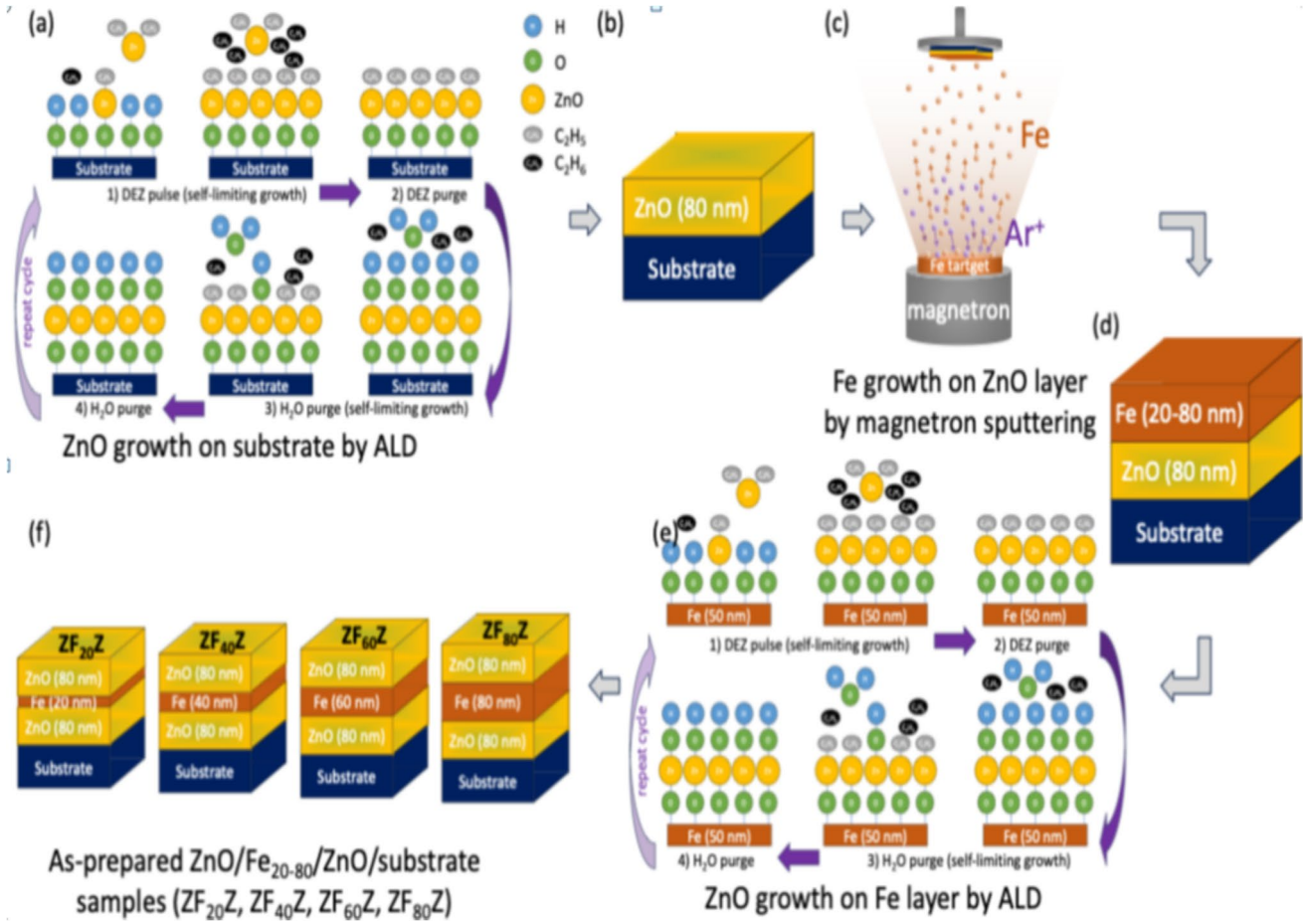

Fig. 1 The steps involved in preparing the sample are as follows: **a** 80-nm ZnO is grown on a substrate using ALD, **b** layer structure after ZnO growth, **c** Fe layer is grown on the ZnO layer in different thicknesses (20, 40, 60, and 80 nm) by magnetron sputtering, **d** layer structure after magnetron sputtering, **e** 80-nm ZnO is grown on top of the magnetron-sputtered Fe layer again by ALD, and **f** layer structure of the prepared samples

using a double-beam spectrophotometer (UV-3101PC Shimadzu).

3 Results and discussion

3.1 Morphological analysis and elemental mapping

The Focused Ion Beam (FIB), of the samples under study previously reported in our earlier publication [22] is briefly presented here to support the current study and to establish comparison and discussion with the present work. As has been clarified in our earlier study, thickness data of $ZF_{20}Z$, $ZF_{40}Z$, $Z_{60}Z$, and $ZF_{80}Z$ seen in Fig. 2a–d, are in excellent agreement with what we wanted to produce. Furthermore, the energy-dispersive X-ray spectroscopy (EDX) results are re-published here to reaffirm the elemental mapping of the prepared thin-film samples as seen in Fig. 2(a_1-d_1). The combination of the above mentioned two techniques, although their results had been previously published in [22, 23], were revisited in the present study to ensure a comprehensive understanding of both the structural integrity and the chemical composition, thereby strengthening the reliability of the obtained results.

3.2 Optical analysis

The optical properties of $ZF_{20}Z$, $ZF_{40}Z$, $ZF_{60}Z$, and $ZF_{80}Z$ were analyzed using UV spectrophotometer with a wavelength range of 200 to 800 nm. Figure 3a,

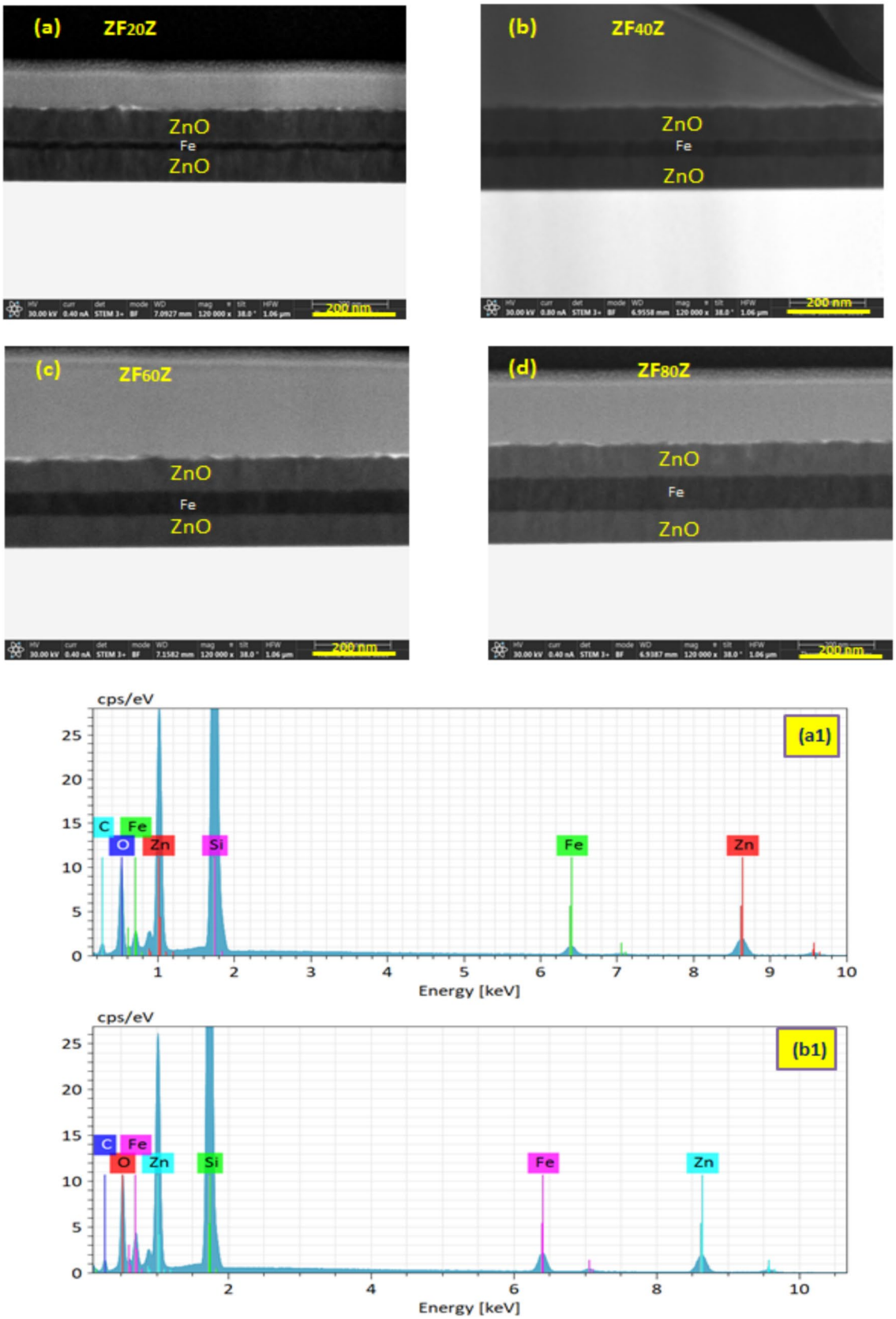

Fig. 2 **a-d** Cross-section electron micrograph and $\mathbf{a_1}$-$\mathbf{d_1}$ EDX spectra of ($ZF_{20}Z$, $ZF_{40}Z$, $ZF_{60}Z$, and $ZF_{80}Z$) thin films, respectively

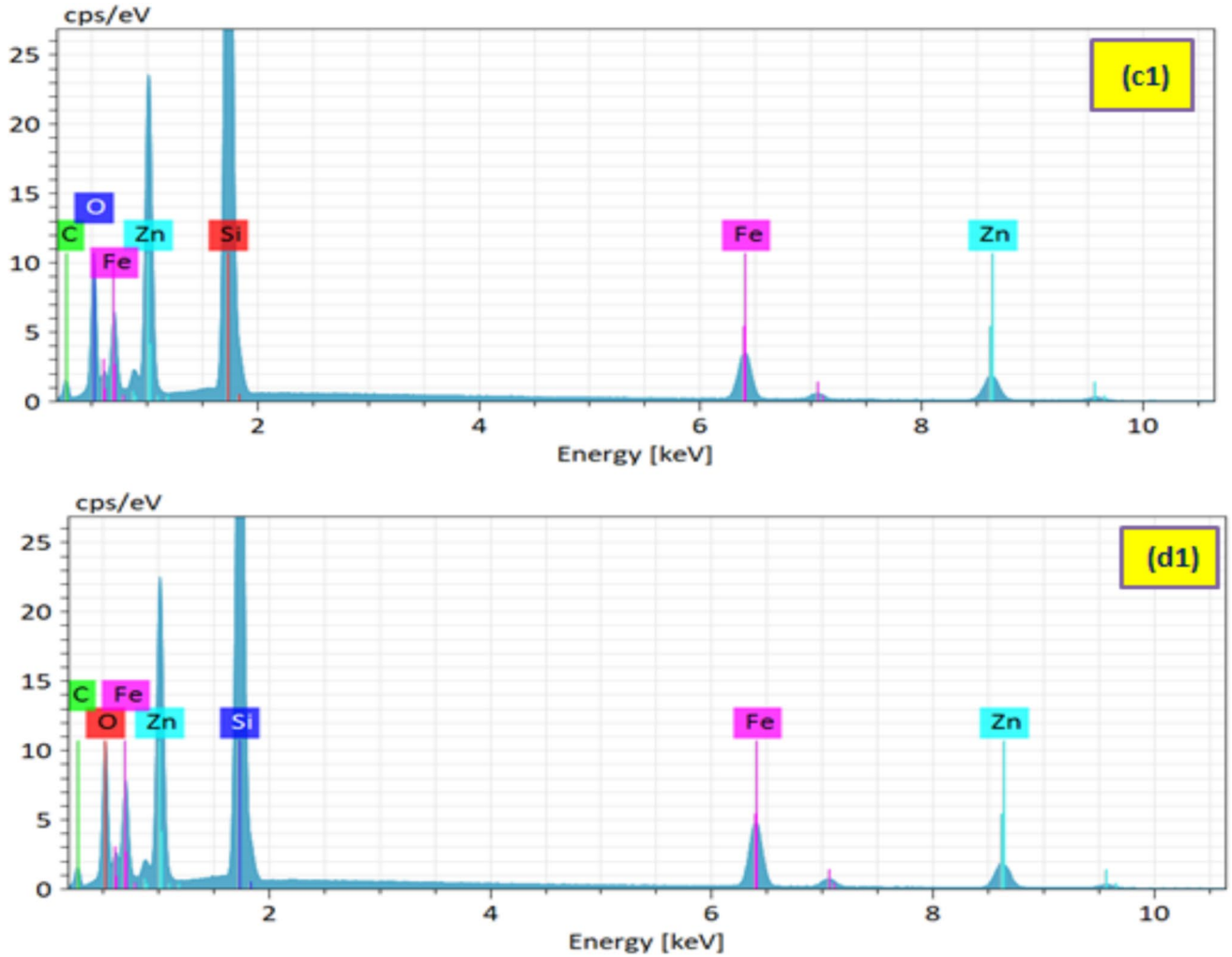

Fig. 2 continued

b displays transmittance and reflectance spectra of the four thin film samples under study.

The transmittance measurement seen in Fig. 3a showed that at wavelength around 390 nm, the four thin films under study have a maximum transmittance of roughly 98%, 92%, 78% and 72% for ZF_{20}, ZF_{40} Z, ZF_{60}Z, and ZF_{80}Z, respectively, indicating the decrease of the transmittance with the increase of the thickness of Fe in ZnO/Fe/ZnO thin-film system, while the observed behavior of the reflectance seen in Fig. 3b of the four thin-film samples of the ZnO/Fe/ZnO system increases at $\lambda \geq 390nm$, with the increase of Fe content. The detected behavior means that light cannot go through the thin-film sample in a significant way, which is in good agreement with the above given results of the transmittance as well. This trend confirms the role of the presence of iron on the optical properties of ZnO thin film. The refractive index **(n)** and the extinction coefficient (*k*), play an important role in selecting the appropriate materials that are suitable for the fabrication of particular optoelectronic applications. The values of the refractive index *(n)*, and the extinction index or the absorption index *(k)* of ZF_{20}Z, ZF_{40} Z, ZF_{60}Z and ZF_{80}Z thin films, can be calculated using Murmann's exact equations for reflectance *(R)* and transmittance *(T)* using the given relations [24, 25]:

$$R = \frac{Ae^{\beta} + Be^{-\beta} + 2C\cos\alpha + 4D\sin\alpha}{Ee^{\beta} + Fe^{-\beta} + 2G\cos\alpha + 4H\sin\alpha} \quad (1)$$

$$T = \frac{16n_0n_g\left(n^2 + K^2\right)}{Ee^{\beta} + Fe^{-\beta} + 2G\cos\alpha + 4H\sin\alpha} \quad (2)$$

where

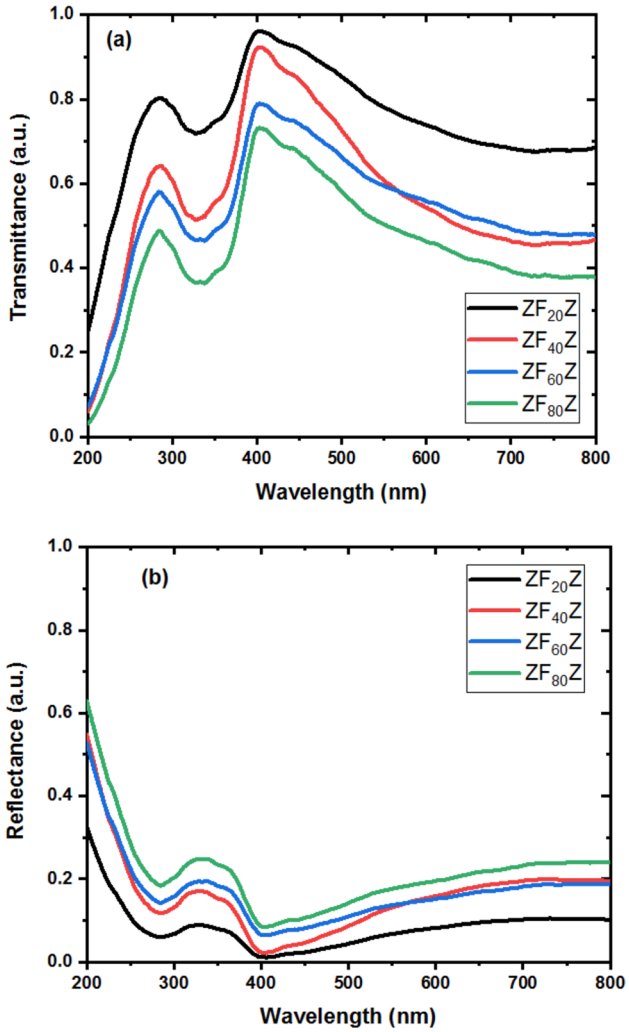

Fig. 3 **a**, **b** Variation of the transmittance and reflectance of the spectral for ($ZF_{20}Z$, $ZF_{40}Z$, $ZF_{60}Z$, and Z F_{80} Z) thin films, respectively, as a function of wavelength

$$A = \left[(n-n_0)^2 + k^2\right]\left[(n+n_s)^2 + k^2\right]$$

$$B = \left[(n-n_s)^2 + k^2\right]\left[(n+n_0)^2 + k^2\right]$$

$$C = \left(n^2+k^2\right)\left(n_0^2+n_s^2\right) - \left(n^2+k^2\right)^2 - n_0^2 n_s^2 - 4n_0 n_s k^2$$

$$D = K(n_s - n_0)(n^2 + k^2 + n_0 n_s)$$

$$E = \left[(n+n_0)^2 + k^2\right]\left[(n+n_s)^2 + k^2\right]$$

$$F = \left[(n-n_0)^2 + k^2\right]\left[(n-n_s)^2 + k^2\right]$$

$$G = \left(n^2+k^2\right)\left(n_0^2+n_s^2\right) - \left(n^2+k^2\right)^2 - n_0^2 n_s^2 - 4n_0 n_s k^2$$

$$H = K(n_s + n_0)(n^2 + k^2 - n_0 n_s)$$

Here, (n_s) is the refractive index of substrate and (n_o) is the refractive index of air. Murmann's exact Eqs. (1) and (2) are solved simultaneously to obtain the accurate values of (n) and (k) using a special iterative computer program.

The results disclose that the induced Fe thickness changes both (n) & (k) of the four thin-film samples. The higher the Fe content, the greater the number of charge carriers that are introduced into ZnO, which will lead to an increase in the index of refraction as observed in Fig. 4a, b. Furthermore, the observed trend is further supported by bang gap narrowing as seen in [22], and the interface polarization effects at the ZnO/Fe boundaries that also play minor role. Therefore, the increase in (n)&(k) in the ZnO/Fe/ZnO system with the increase of Fe interlayer thickness demonstrates its suitability for various optical applications such as optical coatings with tailored anti-reflective properties. Moreover, it can enhance the efficiency of photovoltaic devices through optimizing of the Fe interlayer thickness and can also be utilized in the development of optical data storage systems. The observed increase in (k) further suggests the potential of this structure for optical sensors applications. The values of (n) & (k) were used to calculate the reflectivity (R_{ref}). Reflectivity quantifies the behavior of light when interacting with the surfaces. Reflectivity can be obtained using the formula given in Eq. (3) [26].

$$R_{ref} = \frac{[(n-1)^2 + k^2]}{[(n+1)^2 + k^2]} \tag{3}$$

The dependence of $(\boldsymbol{R_{ref}})$ versus wavelength for $ZF_{20}Z$, $ZF_{40}Z$, $ZF_{60}Z$ and $ZF_{80}Z$, are shown in Fig. 4c. It can be seen that all the $(\boldsymbol{R_{ref}})$ curves corresponding to the change of Fe thickness in ZnO/Fe/ZnO system decreases with the decrease of Fe thickness. It should be noted that in case of layered materials, $(\boldsymbol{R_{ref}})$ is a phenomenological indicator of the interaction between layers such as interference effects, multiple

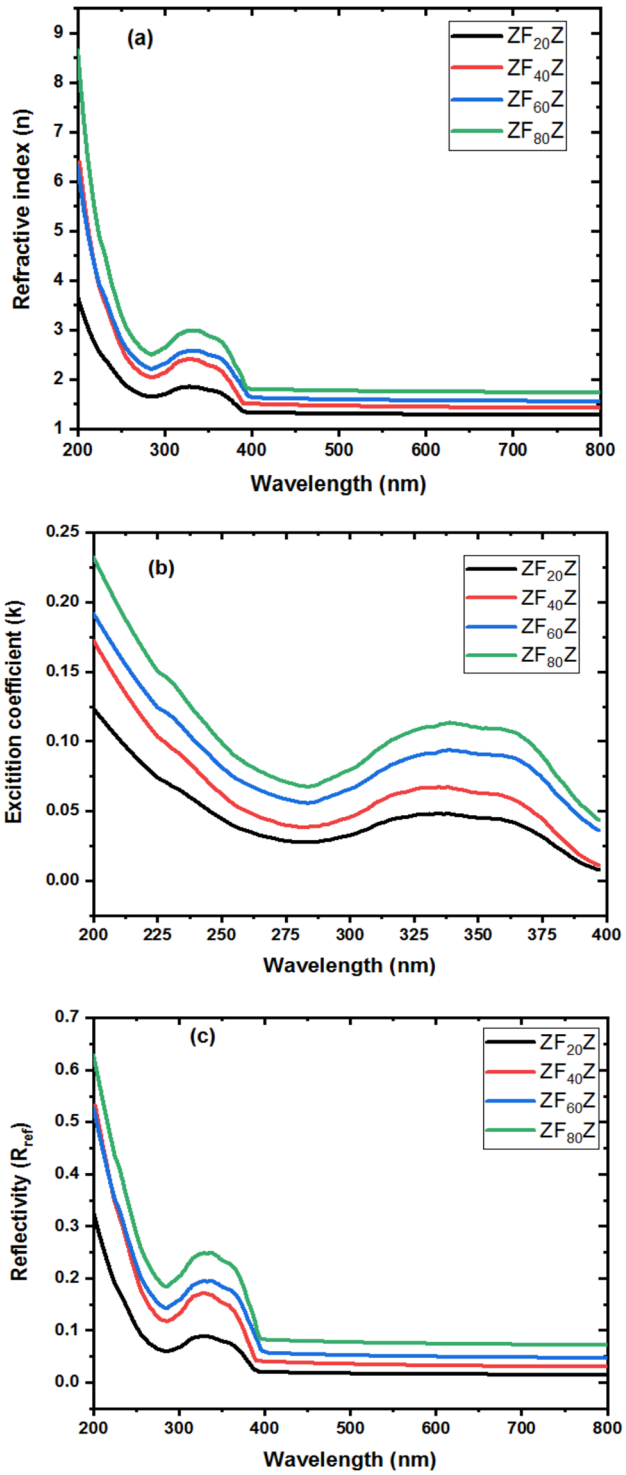

Fig. 4 **a–c** An illustration of n, k, and R_{ref} versus wavelength (λ) for different multilayer thin films ($ZF_{20}Z$, $ZF_{40}Z$, $ZF_{60}Z$, and Z F_{80} Z), respectively

reflection and interface roughness. Reflectivity can reveal information about the refractive index and extinction coefficient, and it is a measure of the intrinsic reflectance of the thin film at the surface, whereas the reflectance considers other factors present behind the surface of the layer thin film under study such as layer thickness composition, interface roughness, and optical properties. Figure 4a and c shows that the material with the highest *(n)* value also has the highest *(R)* value.

3.3 Dielectric constants

The study of the dielectric constant obtained from optical dispersion parameters *(n&k)*, provides valuable insight into the interaction between electromagnetic radiation and the electronic structure of materials**.** The dielectric constant, which consists of real and imaginary components, is directly related to the refractive index and extinctions coefficient obtained from optical analysis. Throughout the evaluation of these optical dispersion parameters, important information about the polarization ability, energy band structure and loss mechanism of the material can be revealed. The complex dielectric ($\boldsymbol{\varepsilon}^*$) provides valuable insight into the optical response of the material. The dielectric materials are used in many applications such as sensors and circuit components. In oxide materials, the complex dielectric constant ($\boldsymbol{\varepsilon}^*$) is utilized by the Eq. (4) [27].

$$\varepsilon^* = \varepsilon_1 + \varepsilon_2 \tag{4}$$

where ($\boldsymbol{\varepsilon}_1$) is the real part of the electronic dielectric constant, which is associated with the polarization of the medium and represents how much electric energy, can be stored, when subjected to an external electric field. It mainly influences the refractive index and determines how light propagates through the film. In contrast ($\boldsymbol{\varepsilon}_2$), the imaginary part of electronic dielectric constant corresponds to the energy dissipation or absorption within the material and is related to the losses arising from free carrier absorption, therefore, an increase in ($\boldsymbol{\varepsilon}_2$) indicates enhanced optical absorption or dielectric loss. The real and imaginary parts of the dielectric constants were determined using the following relations [28].

$$\varepsilon_1 = n^2 - k^2 \tag{5}$$

and

$$\varepsilon_2 = 2nk \tag{6}$$

The graphical presentation of $(\boldsymbol{\varepsilon_1})$ and $(\boldsymbol{\varepsilon_2})$ as a function of the photon energy $(\boldsymbol{h\,\upsilon})$ for the four thin-film samples under study are given in Fig. 5a, b.

From Fig. 5a, b, the variation of $(\boldsymbol{\varepsilon_1})$ and $(\boldsymbol{\varepsilon_2})$ with Fe incorporation in ZnO/Fe/ZnO thin film system, thus reveals the influence of the interlayer on the electronic polarizability and light-matter interaction in the ZnO-based structure, which in turn increases both parts of the dielectric constants that can be beneficial for energy storage applications. The dissipation factor or loss factor *tanδ* signifies the amount of loss in power and is usually observed via heating. The *tanδ* is a measure of the loss of energy that goes into heating a dielectric material in a varying electric field and is the tangent of the angle between the alternating field and the material loss component. Therefore, the dissipation factor can be expressed in terms of $(\boldsymbol{\varepsilon_1})$ & $(\boldsymbol{\varepsilon_2})$ by the following Eq. (7) [29].

$$\tan\delta = \frac{\varepsilon_2}{\varepsilon_1} \tag{7}$$

The variation of $\boldsymbol{tan\delta}$ as a function of $(\mathbf{h}\ \boldsymbol{\upsilon})$ for $ZF_{20}Z$, $ZF_{40}Z$, $ZF_{60}Z$ and $ZF_{80}Z$ thin films is revealed in Fig. 5c. As observed, the value of *tanδ* was found to increase with the increase of Fe interlayer thickness from 20 to 80 nm. The interface between the Fe interlayer and the surrounding materials can lead to an increase in dielectric loss. The increase in tangent loss $\boldsymbol{tan\delta}$ at low photon energy is mainly attributed to the space charge polarization effect. The incorporation of Fe introduces additional defects, which enhance charge carrier hopping and trapping

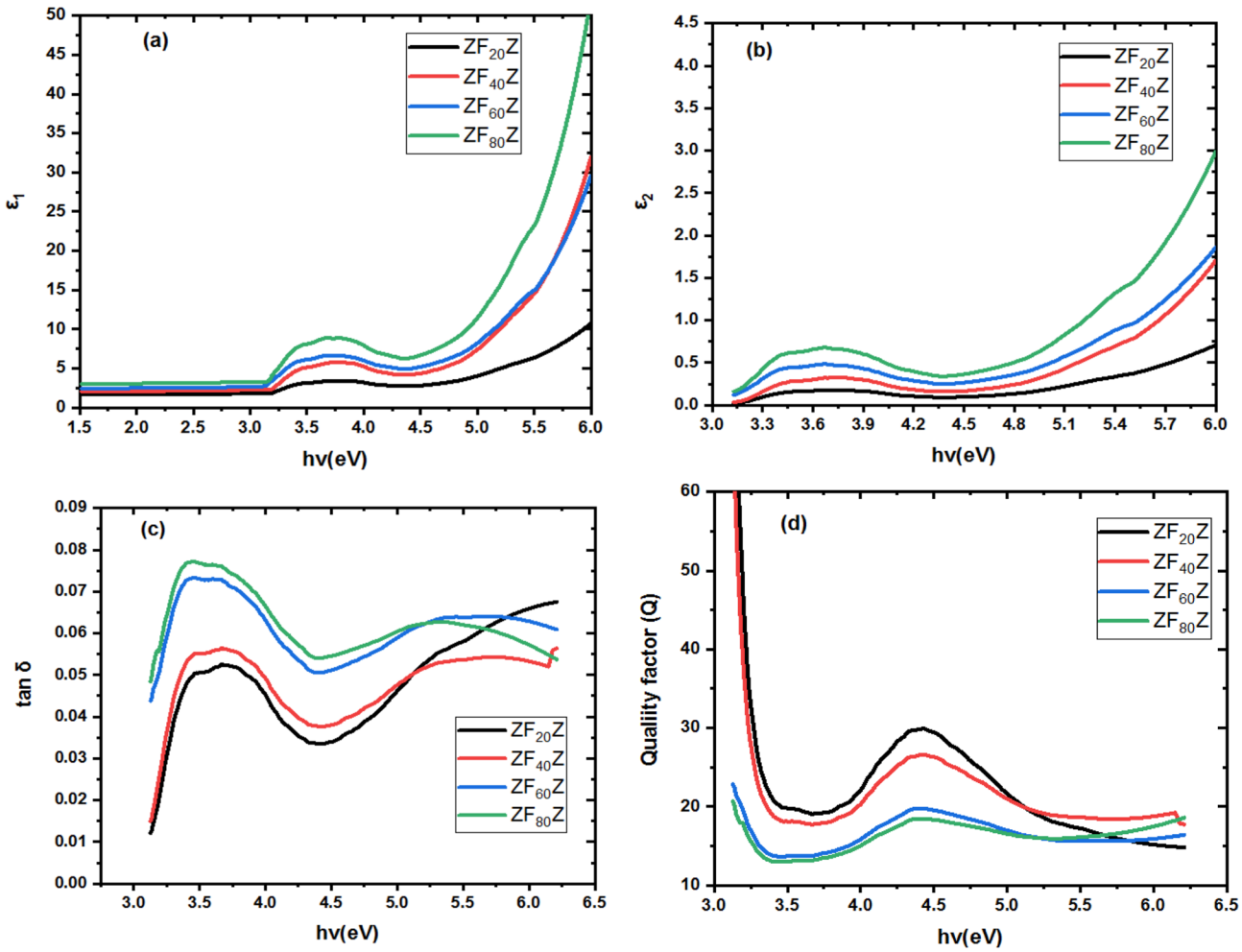

Fig. 5 **a–d** A graphical representation of the dielectric parameters(ε_1&ε_2), tan δ, and Quality factor (Q) against (hν) of different multilayer thin films ($ZF_{20}Z$, $ZF_{40}Z$, $ZF_{60}Z$, and $Z\,F_{80}\,Z$), respectively

at grain boundaries. These localized relaxation processes lead to greater energy dissipation, resulting in a higher loss factor at low photon energy. As photon energy increases, charge carriers gain sufficient energy to overcome localized barriers and move more freely through the lattice, thereby reducing charge accumulation and interfacial polarization. Consequently, ***tanδ*** gradually decrease in the high-energy region due to the diminished relaxation losses. Such behavior can only be observed in oxide materials, which means that the Fe interlayer in ZnO/Fe/ZnO is useful for photovoltaics and high-frequency devices applications and can be beneficial for RF devices such as antennas and resonators, where high dielectric constants and dielectric loss are desired. This means that the thickness of the Fe interlayer should be optimized to achieve the desired dielectric constants and dielectric loss [30]. The Quality factor or *(Q)* factor is a dimensionless parameter that can be defined as Q = 1 / tanδ. *(Q)* is reciprocal of the dielectric tangent. Figure 5d represents the *(Q)* factor of the four thin-film samples under study versus photon energy. An overview of the quality factor of the four thin-film samples under study shows a reduction in *(Q)* with increasing Fe content, this means that as the quality factor decreases the slower decay mode becomes stronger, and energy is stored better in the circuit. The real part of the dielectric constants (ε_1) is related to (λ^2) according to the following Eq. (8) and (9) [31].

$$\varepsilon_1 = n^2 - k^2 = \varepsilon_\infty - B\lambda^2 \tag{8}$$

$$B = \left(\frac{e^2}{4\pi^2\varepsilon_o c^2}\right)\left(\frac{N}{m^*}\right) \tag{8}$$

where (ε_∞) is the infinite high-frequency dielectric constant, ***(e)*** is the electronic charge, (ε_o) is the free space permittivity (8.845×10^{-12}F/m), ***(c)*** is the velocity of light, and (N/m^*) is the ratio of the carrier concentration to the effective mass. Figure 6 shows the graphical presentation of (ε_1) versus (λ^2) for $ZF_{20}Z$, $ZF_{40}Z$, $ZF_{60}Z$, and $FZ_{80}Z$.

Through the graph, the ratio of the carrier concentration to the effective mass (N/m^*) can be obtained from the slope, while the infinite high-frequency dielectric constant (ε_∞) can be obtained from the linear part of this dependence when extrapolated to zero wavelength (λ = Zero). Values of (ε_∞) and $(N/m.^*)$ for the four samples of the ZnO/Fe/ZnO system are listed in Table 1

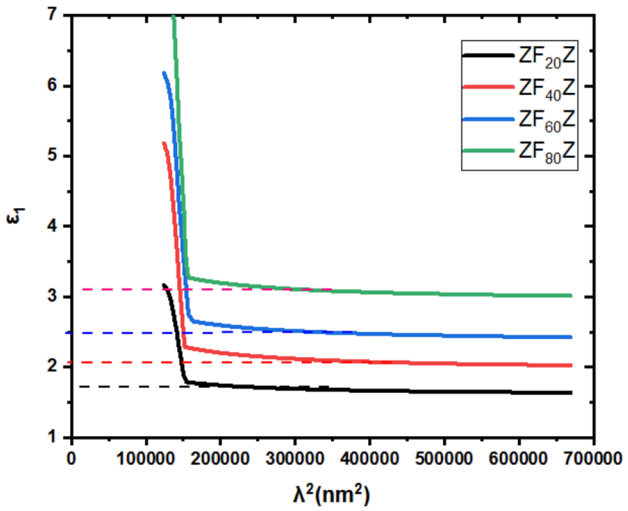

Fig. 6 Variation of ε_1 against λ^2 for different multilayer thin films ($ZF_{20}Z$, $ZF_{40}Z$, $ZF_{60}Z$, and $Z\,F_{80}\,Z$), respectively

The complex real electrical modulus (M^*), define as the inverse of complex relative permittivity. The complex electrical modulus emphasizes the grain boundary conduction mechanism and is useful for conductivity. Thus, the complex electrical modulus can be a significant powerful tool for analyzing dielectric behavior of any material. The (M^*) can be imitative from the dielectric constant and dielectric loss according to the following relation [32].

$$M^* = \frac{\varepsilon_1}{\left(\varepsilon_1^2 + \varepsilon_2^2\right)} \tag{10}$$

Figure 7 shows the complex real electrical modulus (M^*) versus $(h\,\upsilon)$, for the four thin-film samples under investigation.

It is observed that at lower photon energy region the magnitude of (M^*) decreases with the increase of photon energy and the Fe interlayer thickness in the ZnO/Fe/ZnO thin-film system. It is also noticed that the position of the complex real electrical modulus peak occurs at the same photon energy, for the four thin-film samples under study, which means that the process is long-range movement of charge carriers as proposed by [33].

Table 1 A computed values of optical parameters for different multilayer thin films of the ZnO/Fe/ZnO system

Sample	ε_∞	$N/m^*\times10^{55}$ ($m^{-3}.kg^{-1}$)	n_0	E_o(eV)	E_d(eV)	$\chi^{(3)}\times10^{14}$ esu	$n_2\times10^{13}$ esu
$ZFe_{20}Z$	1.71	18.04	1.31	5.69	3.90	0.15	0.44
$ZFe_{40}Z$	2.13	21.15	1.46	5.47	6.09	1.04	2.70
$ZFe_{60}Z$	2.54	23.59	1.60	5.61	8.91	4.33	10.16
$ZFe_{80}Z$	3.12	25.56	1.70	5.51	10.59	9.34	20.59

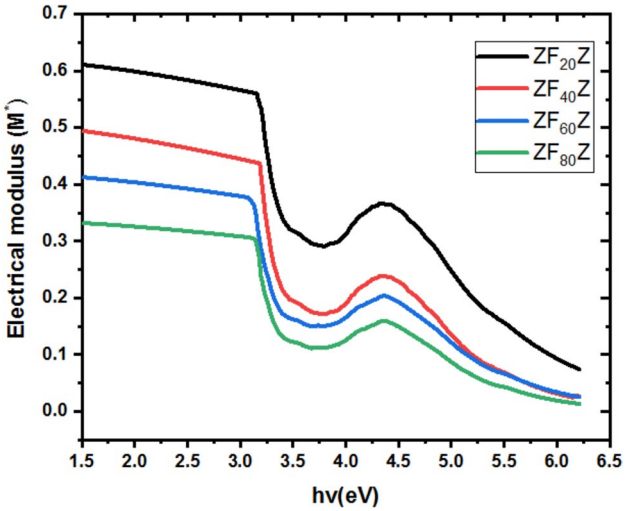

Fig. 7 Variation of M^* against photon energy for the four thin-film samples ($ZF_{20}Z$, $ZF_{40}Z$, $ZF_{60}Z$, and ZF_{80} Z), respectively

3.4 Optical and electrical conductivities

Optical conductivity is used to study the electronic states of any material under investigation. In addition, the optical response of any material is most conveniently studied in terms of the optical and electrical conductivity. Furthermore, optical conductivity is an essential optical parameter that elucidates the charge-transfer complex that exists between the Fe interlayer and the ZnO/Fe/ZnO. The optical conductivity (σ_{opt}) and the electrical conductivity (σ_{elec}) can be detected from the experimental measurements of the optical constants ($n\&k$) and the calculated values of the dielectric constants ($\varepsilon_1\&\varepsilon_2$) and can be determined using the following relations [34, 35].

$$\sigma_{opt.} = \omega\varepsilon_2 \in_0 \tag{11}$$

$$\sigma_{elec.} = \omega\varepsilon_1 \in_0 \tag{12}$$

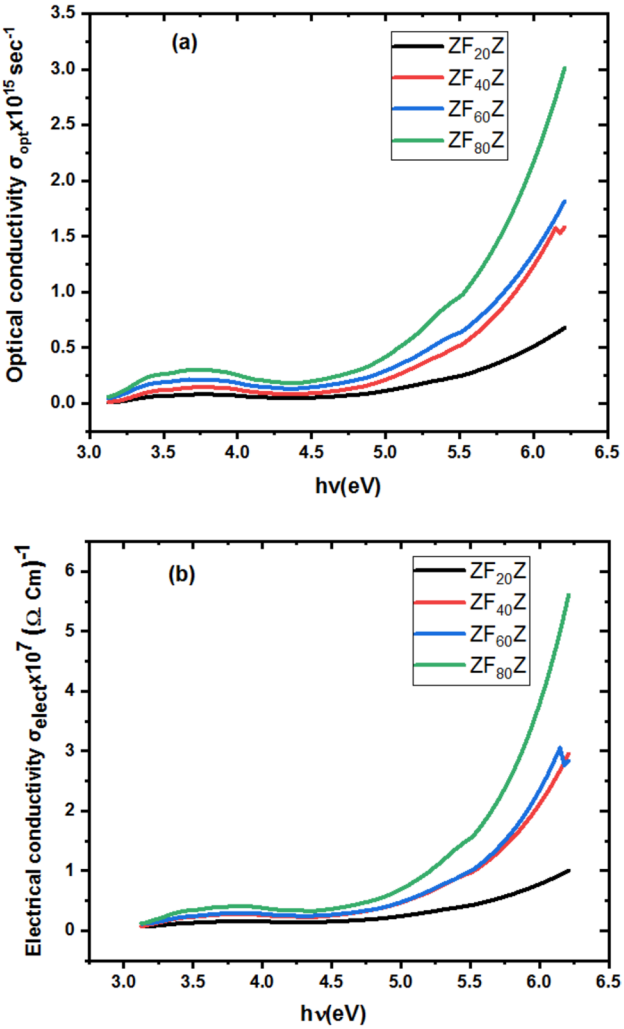

Fig. 8 **a**, **b** Optical and electrical conductivity versus (hν) for the four thin-film samples ($ZF_{20}Z$, $ZF_{40}Z$, $ZF_{60}Z$, and ZF_{80} Z) respectively

where $\omega = 2\ \pi\ f$ (f is the frequency $f = c/\lambda$), c is the velocity of light, λ is the wavelength, and ε_o is the vacuum permittivity. Figure 8a, b presents the optical and electrical conductivities for the four thin film samples under investigation.

As seen in Fig. 8a, b the optical conductivity and electrical conductivity were found to increase as the photon energy, and the thickness of the Fe interlayer increases by providing pathway for charge carriers, and can contribute to an increase in dielectric loss as seen in Fig. 5c. The improvement observed with the raise in Fe thickness is due to the higher charge carrier concentration, which enhances the material electrical and optical performance as seen in Table 1. The incorporation process of Fe with ZnO indicate a positive influence that improves the mechanism of charge conduction for the charge-transfer process that leads to the increase of the optical and electrical conductivies.

3.5 Wemple–DiDomenico (WDD) model

The Wemple–DiDomenico *(WDD)* model provides a reliable and strightforward approach for analyzing the optical dispertion of dielectric and semiconductor materials. It offers better accuracy and simplicity comared with other models, such as Sellmeier and Drude, and it is particularly suitable for multilayer system like ZnO/Fe/ZnO, where muliple interfaces influence the optical response. According to the *(WDD)* model the optical data could be described to an excellent approximation by the ensuring relation [36].

$$\left(n^2-1\right)^{-1}=\frac{\left[E_o^2-(h\nu)^2\right]}{E_oE_d} \tag{13}$$

where (E_o) is the single oscillator energy and $(\boldsymbol{E_d})$ is the dispersion energy. The experimental validation of Eq. (13) can be defined by plotting $\mathbf{(n^2\text{-}1)^{-1}}$ versus $\boldsymbol{(h\nu)^2}$ (see Fig. 9). The value of the static refractive index $(\boldsymbol{n_o})$ is determined by extrapolating the ***(WDD)*** dispersion equation to $(h\upsilon > 0)$**,** while the values of $\boldsymbol{(E_o)}$ and $\boldsymbol{(E_d)}$ can be determined directly from the slope $(E_oE_d)^{-1}$ and the interception on the vertical axis (E_o/E_d). The values of (n_o), (E_o), and (E_d) are given in Table 1.

The validity of the applicability of the relation given in Eq. (13), has been achieved by the linear behavior of the given curves for the four thin film samples under study. The nonlinear refractive index is intensity dependent index of refraction. The nonlinear refractive index $\boldsymbol{(n_2)}$ is deduced on the basis of the linear refractive index and can be expressed using the empirical relation [37].

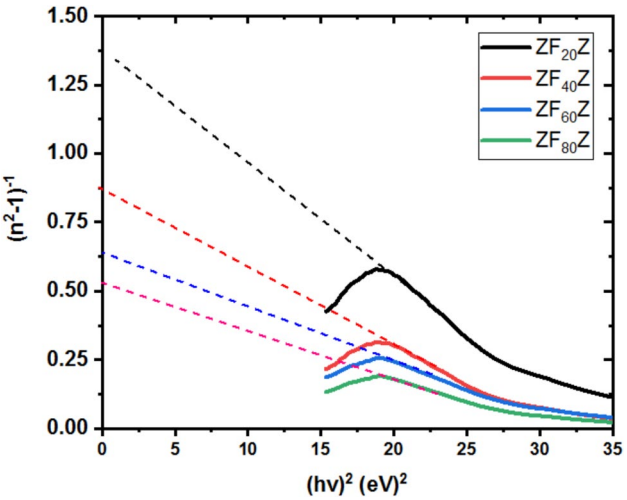

Fig. 9 Graphical presentation of $(n^2\text{-}1)^{-1}$ against $(h\nu)^2$ for the four thin-film samples ($ZF_{20}Z$, $ZF_{40}Z$, $ZF_{60}Z$, and Z F_{80} Z) respectively

$$n_2=\frac{12\pi\chi^{(3)}}{n_o} \tag{14}$$

where $\chi^{(3)}$ is the third order of nonlinear susceptibility, and (n_o) is the static refractive index. $\chi^{(3)}$ is given by [38]:

$$\chi^{(3)}=\frac{B}{(4\pi)^4}\left(n_o^2-1\right)^4=\frac{B}{(4\pi)^4}\left(\frac{E_d}{E_o}\right)^4 \tag{15}$$

where the constant $\boldsymbol{B}=1.7\times10^{-10}$ in (esu). Values of $\chi^{(3)}$ and $(\boldsymbol{n_2})$, are calculated and tabulated also in Table 1. The present studies revealed that the insertion of an appropriate amount of metallic layer Fe between two layers of ZnO allows the increase of the nonlinear refractive index, this increase can enhance nonlinear effects that can be used to improve optical switching devices and can also increase the sensitivity of optical devices such as sensors and detectors. An increase in nonlinear optics can be useful for improving the optical signal devices such as optical filters and optical amplifiers, while also helping to understand the behavior of quantum systems, develop new quantum information for processing techniques, and enable innovative applications in various fields.

4 Conclusion

In this study, we investigated the influence of Fe interlayer thickness on the optical dispersion parameters, dielectric constant, optical and electrical conductivity, and reflectivity of ZnO /Fe/ZnO thin films prepared by ALD and DC-magnetron sputtering techniques. The structural and compositional analysis (EDX) and the cross-section (FIB) confirmed the well -defined multilayer formation with controlled thickness. The optical results revealed that increasing Fe thickness leads to a rise in refractive index, extinction coefficient, and optical and electrical conductivity, accompanied by higher dielectric loss and dissipation factors at low photon energy. These variations suggest an increase in free carrier concentration and enhanced light absorption with Fe incorporation. Moreover, the increase in Fe content improves optical and electrical conductivity, demonstrating its positive effect on charge transport and its potential use in optoelectronic devices, such as solar cells and LEDs. The analysis based on the Wemple–DiDomenico *(WDD)* model showed an increase in nonlinear refractive index with Fe addition suggesting the suitability of these films for nonlinear optical and photonic applications. Overall, Fe interlayer modification offers an effective way to tune the optical and dielectric performance of ZnO-based multilayer system for multilayer device applications.

Acknowledgements

This work was prepared at the University of Debrecen, Hungary, according to the agreement between the Faculty of Education, Ain Shams University "Coordinator and Supervisor *Prof. Dr. Suzan S. Fouad* and the Faculty of Science and Technology, the University of Debrecen" Coordinator and Supervisor *Prof. Dr. Zoltán Erdélyi*. The optical parameters were measured at the central lab of the physics department at the Faculty of Education at Ain Shams University. Project no. TKP2021- NK TA-34 has been implemented with the support provided by the National Research, development, and Innovation Fund of Hungary, financed under the TKP2021-NKTA funding scheme, supported by the University of Debrecen Program for Scientific publication.

Author contributions

S.S. Fouad:—The idea and the writing and the revision. Eszter Baradács, G.Katona, G. Vecsei:—Prepared samples and made the characterizations. A.E.Bekheet:- Calculated the different parameters and prepared the results. M.Nabil:- Prepared all the figures, in the final form and responsible for the correspondence. Zoltán Erdélyi:—Prepared and supervising all the characteristics that had been made in Debrecen.

Funding

Open access funding provided by The Science, Technology & Innovation Funding Authority (STDF) in cooperation with The Egyptian Knowledge Bank (EKB).

Data availability

All data generated or analyzed during this study are included in this published article.

Declarations

Competing interest The authors declare no competing interests.

References

1. S.S. Fouad, M. Nabil, B. Parditka, A.M. Ismail, E. Baradács, H.E. Atyia, Z. Erdélyi, Assessing, surface morphology, optical, and electrical performance of ZnO thin film using ALD technique. J. Nanopart. Res. **25**(8), 172 (2023)
2. S. Sriram, A. Thayumanavan, Optical and electrical properties of nitrogen doped ZnO thin films prepared by low cost spray pyrolysis technique. J. Electron Devices **15**, 1215–1224 (2012)
3. H. Zaka, B. Parditka, Z. Erdélyi, H.E. Atyia, P. Sharma, S.S. Fouad, Investigation of dispersion parameters, dielectric properties and opto–electrical parameters of ZnO thin film grown by ALD. Optik **203**, 163933 (2020)
4. M. Sajjad, I. Ullah, M.I. Khan, J. Khan, M.Y. Khan, M.T. Qureshi, Structural and optical properties of pure and copper doped zinc oxide nanoparticles. Results Phys. **9**, 1301–1309 (2018)
5. S.S. Fouad, L.I. Soliman, E. Baradács, M.E. Sayed, B. Parditka, N.F. Osman, M. Nabil, Z. Erdélyi, Advances for enhancing the electrical properties and microhardness activity of ZnO/Cu/ZnO thin films prepared by ALD. J. Mater. Sci. **58**(15), 6632–6642 (2023)
6. F. Lekoui, S. Hassani, E. Garoudja, R. Amrani, W. Filali, O. Sifi, S. Oussalah, Elaboration and characterization of pure ZnO, Ag: ZnO and Ag-Fe: ZnO thin films: effect of Ag and Ag-Fe doping on ZnO physical properties. Rev. Mex. Fis. **69**(5), 0–0 (2023)
7. B. Marzougui, Y.B. Smida, M. Ferhi, H. Ferjani, D. Onwudiwe, A.H. Hamzaoui, M. Triki, Y.A. Douri, Photoluminescence properties of Pr-doped LaAsO4: an experimental and theoretical study employing density functional theory. Ceram. Int. **50**(15), 26435–26445 (2024)
8. B. Marzougui, Y.B. Smida, R. Marzouki, D.C. Onwudiwe, Y. Al-Douri, A.H. Hamzaoui, Combustion synthesis, characterization, and photodegradation performance of La2-xBixCuO4. Solid State Commun. **364**, 115113 (2023)
9. L. Mohamed, M. Noureddine, B. Mokhtar, Y. Al-Douri, B. Djillali, B. Lakhdar, A.F.A. El-Rehim, M. Jadan, Dislocations and crystallite size distribution of cadmium oxide thin films synthesized by spray pyrolysis technique. Mater. Sci. Eng. B **286**, 116055 (2022)
10. Y. Al-Douri, K. Gherab, K.M. Batoo, E.H. Raslan, Detecting the DNA of dengue serotype 2 using aluminium nanoparticle doped zinc oxide nanostructure: synthesis, analysis and characterization. J. Mater. Res. Technol. **9**(3), 5515–5523 (2020)
11. S. Sagadevan, S. Vennila, A.R. Marlinda, Y. Al-Douri, M.R. Johan, J.A. Lett, Synthesis and evaluation of the structural, optical, and antibacterial properties of copper oxide nanoparticles. Appl. Phys. A **125**(8), 489 (2019)
12. A. Bouhemadou, D. Allali, K. Boudiaf, B. Al Qarni, S. Bin-Omran, R. Khenata, Y. Al-Douri, Electronic, optical, elastic, thermoelectric and thermodynamic properties of the spinel oxides $ZnRh_2O_4$ and $CdRh_2O_4$. J. Alloys Compd. **774**, 299–314 (2019)
13. A. Bouhemadou, O. Boudrifa, N. Guechi, R. Khenata, Y. Al-Douri, Ş Uğur, B. Ghebouli, S. Bin-Omran, Structural, elastic, electronic, chemical bonding and optical properties of Cu-based oxides ACuO (A= Li, Na, K and Rb): An ab initio study. Comput. Mater. Sci. **81**, 561–574 (2014)
14. Al-Douri, Yarub, ed. *Metal oxide powder technologies: fundamentals, processing methods and applications*. Elsevier, (2020).
15. Q. Fang, Q. Sun, J. Ge, H. Wang, J. Qi, Multidimensional engineering of nanoconfined catalysis: frontiers in carbon-based energy conversion and utilization. Catalysts **15**(5), 477 (2025)
16. M. Lei, B. Hou, S. Zhang, R. Chang, Y. Ji, K. Chen, J. Sun, C. Liu, G.F. Payne, X. Qu, De novo fabrication of dense collagen matrices with patterned hierarchical structures for corneal stromal tissue repair. Adv. Mater. (2025). https://doi.org/10.1002/adma.202502279
17. Ru. Liu, W. Shen, Data acquisition of exercise and fitness pressure measurement based on artificial intelligence technology. SLAS Technol. (2025). https://doi.org/10.1016/j.slast.2025.100328
18. H. Zhang, Y. Chang, Xu. Yantao, C. Liu, X. Xiao, J. Li, X. Ma, Y. Wang, H. Guo, Design and fabrication of a chalcogenide hollow-core anti-resonant fiber for mid-infrared applications. Opt. Express **31**(5), 7659–7670 (2023)
19. R.A. Mohamed, E. Baradács, H.E. Atyia, P. Pál, M.Y. El-Bakry, G. Katona, S.S. Fouad, Z. Erdélyi, Adaptive learning of prediction and simulation on the influence of Fe thickness on the energy gap of ZnO/Fe/ZnO tri-layer thin films. The European Phys. J. B **98**(7), 156 (2025)
20. M. Zhang, J. Zhou, X. Jiang, Te. Shi, X. Jin, Y. Ren, K. Ji et al., MoS_2 nanozyme–Chlorella hydrogels: pioneering a hepatocellular carcinoma integrative therapy. Adv. Funct. Mater. **35**(12), 2417125 (2025)
21. J. Wei, P. Fan, Y. Huang, H. Zeng, R. Jiang, Wu. Zhengzhi, Y. Zhang, Hu. Zhengxi, (±)-Hypandrone A, a pair of polycyclic polyprenylated acylphloroglucinol enantiomers with a caged 7/6/5/6/6 pentacyclic skeleton from Hypericum androsaemum. Org. Chem. Front. **11**(12), 3459–3464 (2024)
22. M. Nabil, S.S. Fouad, G. Katona, E. Baradács, Z. Erdélyi, Energy gap: refractive index in ZnO/Fe/ZnO multilayer

prepared by ALD and DC. J. Mater. Sci. Mater. Electron. **36**(19), 1195 (2025)
23. S.S. Fouad, E. Baradács, M. Nabil, G. Katona, G. Vecsei, Z. Erdélyi, Investigation of Fe thickness effect on the absorption behavior of ZnO/Fe/ZnO tri-layers thin films. Opt. Mater. **157**, 116403 (2024)
24. A.M. Ibrahim, Some physical properties of vacuum deposited $Cd_{0.5}$ $Zn_{0.5}$ Te ternary solid solution. Vacuum **49**(1), 5–8 (1998)
25. E.A.A. El-Shazly, I.T. Zedan, K.F. Abd El-Rahman, Determination and analysis of optical constants for thermally evaporated PbSe thin films. Vacuum **86**(3), 318–323 (2011)
26. A.A. Al-Ghamdi, W.E. Mahmoud, S.J. Yaghmour, F.M. Al-Marzouki, Structure and optical properties of nanocrystalline NiO thin film synthesized by sol–gel spin-coating method. J. Alloys Compd. **486**(1–2), 9–13 (2009)
27. Moss T S, Burrell G J, Ellis B, Semiconductor opto-electronics New York:Wiley, (1973).
28. S.S. Fouad, G.A.M. Amin, M.S. El-Bana, Physical and optical characterizations of $Ge_{10}Se_{90-}$ xTe_x thin films in view of their spectroscopic ellipsometry data. J. Non-Cryst. Solids **481**, 314–320 (2018)
29. H.E. Atyia, N.A. Hegab, Optical spectroscopy and dispersion parameters of $Ge_{15}Se_{60}X_{25}$ (X= As or Sn) amorphous thin films. Eur. Phys. J. Appl. Phys. **63**(1), 10301 (2013)
30. C. Thomas, T. Odysseas, S. Georgios, E.K. Emmanouil, On the calculation of the quality factor photonic resonant structures'. Optical Express **27**, 14505–14522 (2019)
31. S. Chichibu, T. Azuhata, T. Sota, S. Nakamura, Excitonic emissions from hexagonal GaN epitaxial layers. J. Appl. Phys. **79**(5), 2784–2786 (1996)
32. M.E. Sayed, S.S. Fouad, E. Baradács, L.I. Soliman, N.F. Osman, M. Nabil, Z. Erdélyi, Distinguish the effect of Cu additive on complex electrical (dielectric/impedance) behaviors of ZnO thin films. J. Nanopart. Res. **26**(7), 150 (2024)
33. S.S. Fouad, B. Parditka, M. Nabil, E. Baradács, S. Negm, Z. Erdélyi, Effect of Cu interlayer on opto-electrical parameters of ZnO thin films. J. Mater. Sci. Mater. Electron. **33**(26), 20594–20603 (2022)
34. S. Agarwal, P. Lohia, D.K. Dwivedi, Study of optical parameters of Te (1-x)(GeSe0. 5) Scx (0≤ x≤ 0.15) thin films for optical data storage applications. J. Non-Cryst. Solids **606**, 122199 (2023)
35. H. Yan, B. Yang, X. Zhou, X. Qiu, D. Zhu, H. Wu, M. Li et al., Adsorption mechanism of hydrated Lu (OH) 2+ and Al (OH) 2+ ions on the surface of kaolinite. Powder Technol. **407**, 117611 (2022)
36. S.S. Fouad, E. Baradács, M. Nabil, B. Parditka, S. Negm, Z. Erdélyi, Microstructural and optical duality of TiO_2/Cu/TiO_2 trilayer films grown by atomic layer deposition and DC magnetron sputtering. Inorg. Chem. Commun. **145**, 110017 (2022)
37. S.S. Fouad, E. Baradács, M. Nabil, G. Katona, G. Vecsei, Z. Erdélyi, Investigation of Fe thickness effect on the absorption behavior of ZnO/Fe/ZnO tri-layers thin films. Opt. Mater. (2024). https://doi.org/10.1016/j.optmat.2024.116403
38. S.S. Fouad, B. Parditka, M. Nabil, E. Baradács, S. Negm, H.E. Atyia, Z. Erdélyi, Bilayer number driven changes in polarizability and optical property in ZnO/TiO_2 nanocomposite films prepared by ALD. Optik **233**, 166617 (2021)